Catalysis Today 158 (2010) 481–489

Contents lists available at ScienceDirect

Catalysis Today

journal homepage: www.elsevier.com/locate/cattod

Performance of dynamic oxygen storage capacity, water–gas shift and steam reforming reactions over Pd-only three-way catalysts

Zhiqun Han[a], Jianqiang Wang[a,c], Haijun Yan[a], Meiqing Shen[a,b,*], Jun Wang[a], Wulin Wang[c], Ming Yang[a]

[a] Key Laboratory for Green Chemical Technology of State Education Ministry, School of Chemical Engineering & Technology, Tianjin University, Tianjin 300072, PR China
[b] State Key Laboratory of Engines, Tianjin University, Tianjin 300072, PR China
[c] China Automotive Technology & Research Center, Tianjin 300162, PR China

ARTICLE INFO

Article history:
Available online 25 August 2010

Keywords:
Dynamic oxygen storage capacity
Water–gas shift
Steam reforming
Turnover frequency
Compensation effect

ABSTRACT

The catalytic performances of Pd/CeO_2, $Pd/Ce_{0.67}Zr_{0.33}O_2$, and $Pd/Ce_{0.67}Zr_{0.33}O_2$-Al_2O_3 three-way catalysts are evaluated through dynamic oxygen storage pulses (DOSC), water–gas shift reactions (WGS), and steam reforming reactions (SR). Despite the differences in the morphologies and chemical compositions of the catalysts, the very similar mechanisms over the three samples for the above reactions have been confirmed according to the compensation effect. Oxygen migration ability plays a key role in DOSC activities. The dynamic oxygen storage rates (DOSR) are ordered as: $Pd/Ce_{0.67}Zr_{0.33}O_2$-Al_2O_3 > $Pd/Ce_{0.67}Zr_{0.33}O_2$ > Pd/CeO_2. The synergetic effect of ceria contents, oxygen vacancies, and precious metal dispersion determines the activity of WGS reaction. The orders of light-off temperatures are as follows: WGS-fresh: Pd/CeO_2 < $Pd/Ce_{0.67}Zr_{0.33}O_2$-Al_2O_3 < $Pd/Ce_{0.67}Zr_{0.33}O_2$; WGS-aged: $Pd/Ce_{0.67}Zr_{0.33}O_2$-Al_2O_3 < Pd/CeO_2 < $Pd/Ce_{0.67}Zr_{0.33}O_2$. For SR reactions, oxidized states of palladium particles and less acidity of support oxides can be beneficial. Thus the light-off temperatures are ordered as: SR-fresh: $Pd/Ce_{0.67}Zr_{0.33}O_2$ < Pd/CeO_2 < $Pd/Ce_{0.67}Zr_{0.33}O_2$-Al_2O_3; SR-aged: Pd/CeO_2 < $Pd/Ce_{0.67}Zr_{0.33}O_2$-Al_2O_3 < $Pd/Ce_{0.67}Zr_{0.33}O_2$.

1. Introduction

The increasing care of the global environment demands great efforts in automotive exhaust control technologies. Three-way catalyst (TWC) is able to convert CO, HC, and NO_x simultaneously into carbon dioxide, water, and nitrogen. Therefore, it becomes the most widely applied catalytic material for automotive exhaust control hitherto now [1,2].

Ceria-based materials are one of the key components in TWCs. Oxygen storage capacity (OSC) is a crucial property of ceria-based promoters for TWC. The higher OSC, the wider working ranges of air/fuel for efficient pollution control can be approached. Loss of OSC implies the deactivation of the TWC [1]. Much effort has been done to improve the durability of decent OSC under rapid and repeatable redox cycles and high temperatures conditions [2]. As the first generation of OSC materials, pure ceria has the notorious drawbacks like easy thermal sintering and quick catalytic activity deactivation. As the second generation of key promoters for TWC, ceria-zirconia (CZ) solid solutions with better and more durable OSC performances replaced pure ceria since 1993 [3]. More recently, Di Monte et al. and Morikawa et al. [4,5] introduced alumina into ceria-zirconia as a diffusion barrier to improve the thermal stability of the fine particles. For such the third generation of ceria-based promoters for Pd-only TWC, not only the improved OSC is being investigated, but also the other functions of these materials for TWC catalysis need further understanding.

Regarding the catalytic materials, the role of ceria is not limited to OSC activities in real practice. Ceria can also modify CO oxidation, NO conversions, and low-temperature water–gas shift reactions. Through further investigations of components interactions, it has been confirmed that ceria is able to improve the dispersion of precious metals, bring oxidized states to supported Pd particles, and suppress the phase transition of alumina [1,2]. For all these additional functions, not only the lattice oxygen migration ability should be investigated, but the roles of oxygen vacancies, ceria contents, surface basicity, and the physical chemistry states of precious metal particles need further clarification. Regarding the gaseous reactants, the H_2, O_2, H_2O, and CO_2 are generally present in automotive exhaust. Steam concentration up to 10% in volume plays an important role as an oxidant in TWC reaction networks, which converts CO and HCs by the water–gas shift (WGS) and the steam reforming (SR) reactions respectively. Therefore, both the effects of WGS and SR reactions should be carefully considered in exhaust control. The importance of the combined decent activities in OSC, WGS, and SR for TWCs has been discussed [6–21]. Although the

* Corresponding author at: School of Chemical Engineering & Technology, Tianjin University, Tianjin 300072, PR China. Tel.: +86 22 27892301; fax: +86 22 27892301.
E-mail address: mqshen@tju.edu.cn (M. Shen).

0920-5861/$ – see front matter © 2010 Elsevier B.V. All rights reserved.
doi:10.1016/j.cattod.2010.07.020

fundamental understandings about the three generations of OSC materials, CeO_2, $Ce_{0.67}Zr_{0.33}O_2$, and $Ce_{0.67}Zr_{0.33}O_2$-Al_2O_3 have been much attempted, comprehensive comparisons and mechanism studies on these support oxides' corresponding Pd-only TWCs are still limited. The present work is going to systematically compare the activities of Pd/CeO_2, $Pd/Ce_{0.67}Zr_{0.33}O_2$, and $Pd/Ce_{0.67}Zr_{0.33}O_2$-Al_2O_3 catalysts for OSC, WGS, and SR reactions, and to elucidate the key factors that determine such differences from the view of ceria-related components interactions.

2. Experimental

2.1. Sample preparation

CeO_2, $Ce_{0.67}Zr_{0.33}O_2$, and $Ce_{0.67}Zr_{0.33}O_2$-Al_2O_3 ($Ce_{0.67}Zr_{0.33}O_2$:Al_2O_3 weight ratio = 1:1) were synthesized by citric acid sol–gel method. $Ce(NO_3)_3$ (Zibo Rongruida), $Zr(NO_3)_4$ (Zibo Rongruida) and $Al(NO_3)_3$ (Tianjin Kewei) were used as starting materials, citric acid was added as complex agent, and glycol was used as additive. After continuous stirring for 2 h, the mixed solution was treated at 80 °C overnight to form the sponge yellow gel. Then, the gel was dried at 100 °C for 3 h and milled before calcination. The dried gel was calcined at 500 °C for 5 h to obtain the as-prepared support oxides. The 0.5 wt.% Pd loading was achieved by impregnating support oxides with $Pd(NO_3)_2$ aqueous solutions, followed by calcination at 500 °C for 5 h. These as-prepared samples were called fresh samples, and were designated as Pd/CeO_2, Pd/CZ, and Pd/CZA. Aged samples were obtained by hydrothermally aging the as-prepared catalysts at 1050 °C for 10 h in a 10% steam-air condition, which were designated as Pd/CeO_2a, Pd/CZa, and Pd/CZAa respectively.

2.2. Characterization

The X-ray powder diffraction (XRD) patterns were acquired on X'Pert Pro diffractometer operating at 40 kV and 40 mA with ferrum-filtered Co Kα radiation. The 2θ ranges from 20° to 90° with a 0.03 step size. Diffractometer was calibrated using a standard Si sample. The lattice parameters were calculated according to Bragg's equation $2d \sin\theta = k\lambda$. The average particle size was determined by Scherrer equation. All the calculations were done by Jade 5.0 software.

The specific surface area of the sample was measured by the BET (Brunauer–Emmett–Teller) method, using N_2 adsorption/desorption (Quantachrome NOVA2000) at 77 K.

Precious metal (PM) dispersion was measured by CO chemisorption, which avoids the hydrogen spillover effects in H_2-chemisorption. CO chemisorption measurements were performed in a fixed-bed reactor, and the CO concentration was monitored by a quadrupole mass spectrometer (Hiden HPR20). Samples were preheated in Ar/He to 200 °C, oxidized in O_2/Ar/He at 200 °C for 10 min, and subsequently purged with Ar/He at 200 °C for 20 min. The sample was then reduced in H_2/Ar/He at 200 °C for 2 h, and subsequently purged with Ar/He (keeping at 200 °C for 20 min) to room temperature. The measurements start after the stabilization, 4% CO/Ar/He (1 s) and Ar/He (10 s) were alternately pulsed into the system in sequence. A final apparent equilibrium was approached when the concentration of CO signal was steady and equivalent to its inlet concentration. Saturated adsorbed volumes were thus determined. A chemisorption stoichiometry of CO:PM = 1:1 was assumed. The exposed surface area of precious metal Pd was calculated by assuming a surface area of 7.8 $Å^2$ for each Pd atom. The crystallite sizes of the metals particles were estimated, by using the equation d (nm) = 112/(percentage of metal exposed). It was assumed that the palladium particles were spherical in shape, and have the surface density of 1.27×10^9 atoms/m^2 [10].

2.3. Dynamic oxygen storage capacity measurements

Two types of OSC measurements were conducted, including dynamic CO–He pulses and transient CO–O_2 pulses [6]. Concentrations of CO, O_2, CO_2, Ar, and He in the outlet gas were monitored on-line by Hiden HPR20 quadrupole mass spectrometer. 25 mg sample diluted with 40 mg quartz sand was placed in the heat transfer reactor (10 mm diameter) at a height of 1.5 mm, with additional 4 mm redistributing layers of quartz wool on the two sides of catalysts bed. Flow rate of every pulse is 300 ml min^{-1}. Dead volume of the system was 3.5 ml. Errors induced by residence time and possible CO + O_2 turbulent mixing involved catalytic combustion can be limited to 2% during OSC quantifications. Before both of the testing modes, samples were pre-oxidized under 2% O_2/1% Ar/He atmosphere, and then purged under He until no $^{36}O_2$ signal detected. The two experimental modes are described as follows: (1) Transient oxygen release measurements at 773 K were conducted under consecutive CO (5 s)–He (40 s) conditions. 4% CO/1% Ar/He and He were alternately pulsed for 10 times in sequence. (2) Dynamic CO–O_2 pulses (DOSC) measurements were operated from 473 to 773 K with the interval of 100 K. At each testing temperature, 4% CO/1% Ar/He and 2% O_2/1% Ar/He were pulsed alternately in sequence at the frequency of 0.1 Hz. The simulated plug flows repeated for more than 5 cycles to guarantee the reproducibility of collected response curves.

2.4. Water–gas shift (WGS) reaction analysis

WGS activity tests were conducted in a quartz micro-reactor using the gas mixture of 2% CO + 5% H_2O + N_2 (balance) at space velocity of 50,000 h^{-1}. The catalyst powder (200 mg) was diluted with quartz pellets to the volume of 0.9 ml, and was placed at the bottom of the reactor. A standard test was conducted from room temperature to 600 °C at the heating rate of 10 °C min^{-1}. CO outlet concentrations were determined by an IR analyzer.

2.5. Steam reforming (SR) reaction analysis

SR activity tests were conducted in a quartz micro-reactor using the gas mixture of 0.1% C_3H_8 + 5% H_2O + N_2 (balance) at space velocity of 50,000 h^{-1}. The catalyst powder (200 mg) was diluted with quartz pellets to 0.9 ml, and was placed at the bottom of the reactor. A standard activity test was conducted from room temperature to 600 °C at the heating rate of 10 °C min^{-1}. C_3H_8 outlet concentrations were determined by an IR analyzer.

3. Results and discussion

3.1. Texture analysis

The XRD patterns of all samples are shown in Fig. 1. For fresh samples, the main diffraction peaks represent a fluorite cubic structure, and have shown the decent symmetry. This confirms the formation of ceria-zirconia solid solutions, ceria-zirconia-alumina semi-solid solutions, or micromorphology grains [22]. Compared with Pd/CeO_2, the diffraction peaks of Pd/CZ slightly shift to higher angles due to the incorporation of smaller Zr iron (0.84 Å) into CeO_2 lattice, which is also revealed by the change of lattice parameters listed in Table 1. The absence of the diffraction peaks for Al_2O_3 in Pd/CZA indicates that Al_2O_3 incorporates into the CZ lattice to form the semi-solid solution. Another possibility is that Al_2O_3 particles exist as micromorphology grains that are too small to be detected. The peaks for metallic Pd (40.4° and 41.9°) cannot be detected, because the loading of Pd is low, or/and the dispersion of Pd is high. Pd particles on CZ generally stay as more fine particles, compared

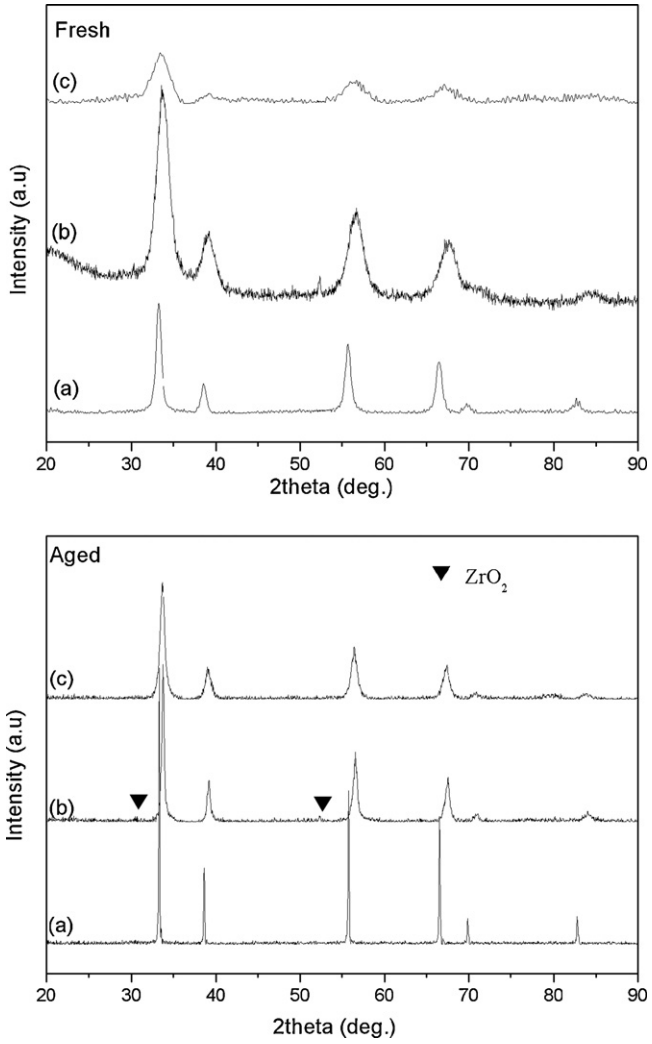

Fig. 1. XRD patterns of (a) Pd/CeO_2, (b) $Pd/Ce_{0.67}Zr_{0.33}O_2$ and (c) $Pd/Ce_{0.67}Zr_{0.33}O_2$-Al_2O_3 in fresh and aged states.

with the situation on Pd/CeO_2 and Pd/CZA. Having higher Pd surface areas and superior thermal stability after hydrothermal aging, CZ supported sample still facilitate Pd dispersion on their interface more than that on CeO_2 and CZA.

The sharpened peaks of the aged samples indicate the larger crystallite sizes. It should be noted that a Zr-rich phase can be identified in the XRD patterns of Pd/CZa sample, while Pd/CZAa sample remains single fluorite lattice structure, without Al_2O_3 or ZrO_2 phases being detected. It suggests that the interaction between CZ and Al_2O_3 can prevent the phase segregation of the CZ and phase transition of Al_2O_3. Therefore, such an interaction is going to improve the thermal stability of the mixed oxides, in agreement with the literatures' findings [4,5,23].

The structural and textural properties of different samples are summarized in Table 1. As indicated by the results of S_{BET} and crystallite size, the hydrothermal ageing treatment induces serious sintering of samples, which is a major driving force for crystal growth. The interaction between CZ and Al_2O_3 prevents the particle sintering. Among the samples, Pd/CZA maintains the smallest particle size. Furthermore, both fresh and aged Pd/CZA show highest surface areas, and the percentage of the specific surface area loss is ordered as: Pd/CeO_2 (95.8%) > Pd/CZ (91.0%) > Pd/CZA (81.6%). However, it should be admitted that the OSC performance and the catalytic activity of ceria-based material do not depend directly on their surface areas. Di Monte et al. reported that the participation of bulk oxygen of ceria-zirconia in reduction may make the high surface areas less important [24].

For Pd supported samples, the dispersion of PM is very important in determining the catalytic activity. According to the research findings of Wang et al. [16], smaller palladium particles expose more active sites at metal–support interfaces, which become beneficial for the adsorption and transference of reactants. In contrast, the surface sites on larger palladium particles are mostly detached from support oxides, which are unfavorable for the catalytic reactions.

As listed in Table 1, all fresh samples have higher PM dispersions and smaller crystallite sizes. After hydrothermal ageing treatment, the decline of the Pd dispersion and the increases of the crystallite size are observed, due to the sintering of palladium particles and agglomeration of support oxides. The decreasing amplitude of precious metal dispersion is as follows: Pd/CeO_2 (90.8%) > $Pd/Ce_{0.67}Zr_{0.33}O_2$-Al_2O_3 (79.6%) > $Pd/Ce_{0.67}Zr_{0.33}O_2$ (75.1%). Concerning the influence of the support composition, two conclusions can be done: (i) pure ceria supports lead to the bigger variations of the precious metal dispersion after hydrothermal aging treatment. The specific surface areas effects should be considered, which physically disperse the Pd components. (ii) conversely, the decreasing amplitude is greatly improved when the support is CZ or CZA. Some electronic metal/support interactions should be considered, which modify the Pd dispersions by controlling the chemical valence and surface bonding of the Pd particles.

3.2. OSC performance

3.2.1. Total OSC with CO–He pulses

To study the total amount of lattice oxygen available under anaerobic atmosphere, CO pulses with He intervals were used to monitor the oxygen migration behavior of the catalysts. Fig. 2 depicts the OSC data in transient CO–He pulses. The amount of produced OSC decreases with increasing number of pulses. TOSC is calculated by adding up the OSCs during the 10 consecutive CO pulses.

Table 1
Surface areas, particle parameters, and Pd dispersions of fresh and aged samples.

Samples	BET (m^2/g)	Lattice parameters[a] (nm)	Particle diameter (nm)	Pd dispersion (%)	Pd surface area (m^3/g Pd)	Pd particle diameter (nm)
Fresh						
Pd/CeO_2	21.8	0.5412 ± 0.00029	15.0	12.5%	6.3	9.0
$Pd/Ce_{0.67}Zr_{0.33}O_2$	30.5	0.5350 ± 000028	4.0	15.4%	7.8	7.3
$Pd/Ce_{0.67}Zr_{0.33}O_2$-Al_2O_3	92.5	0.5414 ± 0.00013	4.6	13.5%	6.8	8.3
Aged						
Pd/CeO_2	0.9	0.5410 ± 0.00011	151.8	1.2%	0. 6	97.5
$Pd/Ce_{0.67}Zr_{0.33}O_2$	2.8	0.5338 ± 0.00017	43.7	3.8%	1.9	29.3
$Pd/Ce_{0.67}Zr_{0.33}O_2$-Al_2O_3	17.0	0.5351 ± 0.00020	14.4	2.7%	1.4	40.8

[a] Lattice parameters are calculated by Jade 5.0, where the experimental errors are provided.

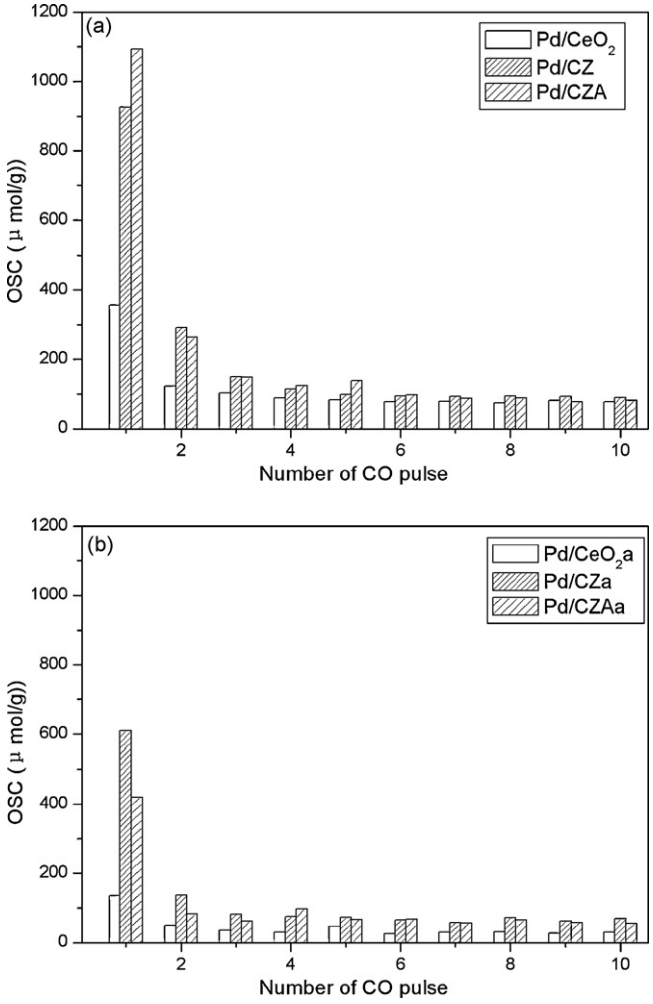

Fig. 2. OSC performance of (a) fresh (b) aged catalysts under consecutive 4% CO/1% Ar/He and pure He at 500 °C.

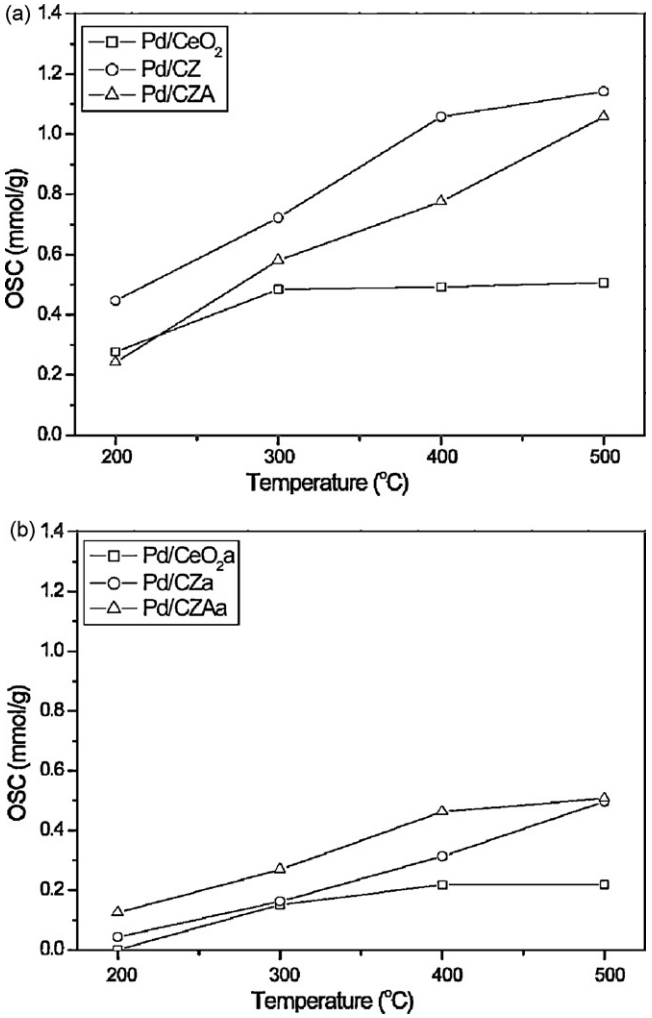

Fig. 3. DOSC values (a) fresh (b) aged different catalysts.

For fresh samples, the TOSC are ordered as: $Pd/Ce_{0.67}Zr_{0.33}O_2$-Al_2O_3 (2205 μmol/g) > $Pd/Ce_{0.67}Zr_{0.33}O_2$ (2050 μmol/g) > Pd/CeO_2 (1150 μmol/g). For aged samples, the order is $Pd/Ce_{0.67}Zr_{0.33}O_2$ (1307 μmol/g) > $Pd/Ce_{0.67}Zr_{0.33}O_2$-Al_2O_3 (1036 μmol/g) > Pd/CeO_2 (446 μmol/g). In line with the previous observation, the values of specific surface areas have limited correlation with the OSC activities [25].

Fig. 2 depicts the timed-resolved oxygen release manners under anaerobic conditions. During initial CO pulses, CO oxidation occurs mostly by using the surface and near-surface oxygen of the catalysts. After the depletion of such a kind of oxygen species, the rest of the CO pulses are mostly oxidized by bulk oxygen in a two-step process, including the adsorption of CO on the catalyst' surface and its subsequent combination with bulk oxygen species. Bulk oxygen migration is the rate-determining step here, which can be considered as a function of the intrinsic structure of the material [26]. A direct relationship between lattice defects and OSC was discussed by Mamontov et al., and they suggest that oxygen defects are the sources of OSC in ceria-based material [27]. Moreover, microstructure variation of ceria-based materials induced by doping with aliovalent oxides, such as ZrO_2 and Al_2O_3, could improve lattice oxygen mobility [28]. This is the primary reason that ceria-zirconia and ceria-zirconia-aluminum are being used in TWC as the improved generations of promoters or support oxides.

Lattice defects have additional functions in OSC process when precious metal is supported on ceria-based materials. Such a kind of Pd–support interactions widely exists in the real application of modern Pd-only TWC [29]. Due to the higher energy potential of the Ce^{4+}/Ce^{3+} redox couple (1.61 eV) than that of the Pd^{2+}/Pd^0 (0.915 eV) redox couple, oxygen vacancies get formed easily and act as the motivator in oxygen spillover and back-spillover processes at PM/CZ interfaces [2]. In this regard, oxygen vacancy is the key factor in bulk oxygen mobility. The synergetic effect of PM and lattice defects further determines the oxygen mobility and diffusion directions.

3.2.2. *Dynamic OSC with CO and O_2 pulses*

The dynamic OSC measurement simulates the real operating conditions, where the exhaust components oscillate between reducing and oxidizing atmosphere in a high frequency. CO reduction and O_2 oxidation have been chosen as the representative model reactions for rich and lean cycles, and the DOSC results are shown in Fig. 3.

Generally, DOSC can be enhanced with increasing reaction temperatures, because higher amount of lattice oxygen becomes available for the reactions and the oxygen spillover processes have been accelerated [6]. At low temperatures (below 300 °C), the surface and near-surface oxygen makes major contribution to DOSC activity. At higher temperatures (above 300 °C), bulk oxygen migration plays an important role to determine the DOSC performance. The bulk oxygen migration capability is promoted by the introduction of Zr and Al, as indicated by the improved

DOSC performances of Pd/CZ and Pd/CZA especially at high temperatures. After hydrothermal ageing treatment, the DOSCs of all samples decline rapidly due to the sintering of PM and agglomeration of support oxides. The DOSC activities are ordered as follows: Pd/CZA > Pd/CZ > Pd/CeO_2 in both fresh and aged states. Thermally stable Pd/CZA also has decent lattice oxygen mobility. In agreement with the research findings of Morikawa et al. [5], the introduction of alumina into CZ solid solution as a diffusion barrier improves the thermal stability and the DOSC performance.

In order to further study the durability of OSC activities for different samples, the loss of OSC designated as OSC_{loss}% is estimated by the following equation: $OSC_{loss}\% = ((OSC_{fresh} - OSC_{aged})/OSC_{fresh}) \times 100$ [30]. The results are listed in Fig. 4. The smaller OSC_{loss}% indicates the better durability of OSC activity. Among all the samples, Pd/CZA exhibits the lowest OSC_{loss}%, demonstrating its decent OSC durability after high temperature thermal treatment.

As suggested by Hori et al. and Jia et al. [31,32], the dynamic oxygen storage rate (DOSR) is defined as the amount of oxygen stored or released in the first second of every lean-rich oscillation

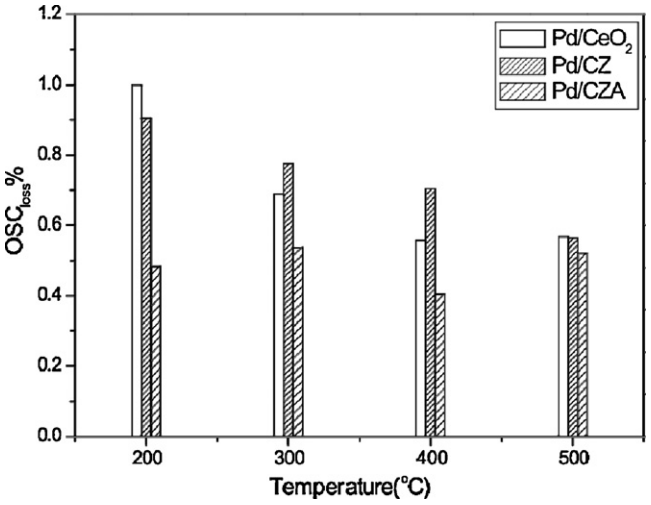

Fig. 4. Percentage of OSC losses for different samples after ageing.

Table 2
DOSRs of fresh and aged Pd supported samples.

Catalysts		DOSR (μmol-O s^{-1} g_{cat}^{-1})			
		200 °C	300 °C	400 °C	500 °C
Pd/CeO_2	Fresh	20.8	32.9	36.2	44.3
	Aged	0	14.9	15.6	27.1
Pd/$Ce_{0.67}Zr_{0.33}O_2$	Fresh	17.9	49.0	41.6	64.4
	Aged	2.3	13.6	22.1	23.5
Pd/$Ce_{0.67}Zr_{0.33}O_2$-Al_2O_3	Fresh	27.5	33.8	60.1	72.3
	Aged	6.3	25.1	35.9	78.6

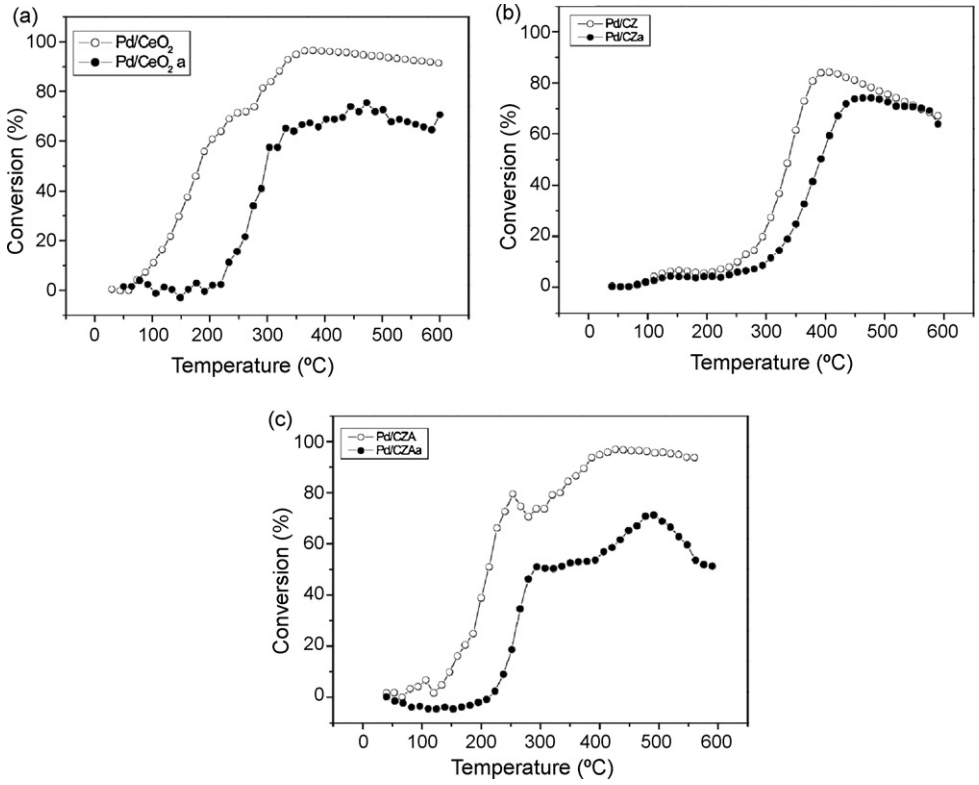

Fig. 5. Conversion profiles of water–gas shift over (a) Pd/CeO_2, (b) Pd/$Ce_{0.67}Zr_{0.33}O_2$ and (c) Pd/$Ce_{0.67}Zr_{0.33}O_2$-Al_2O_3 catalysts.

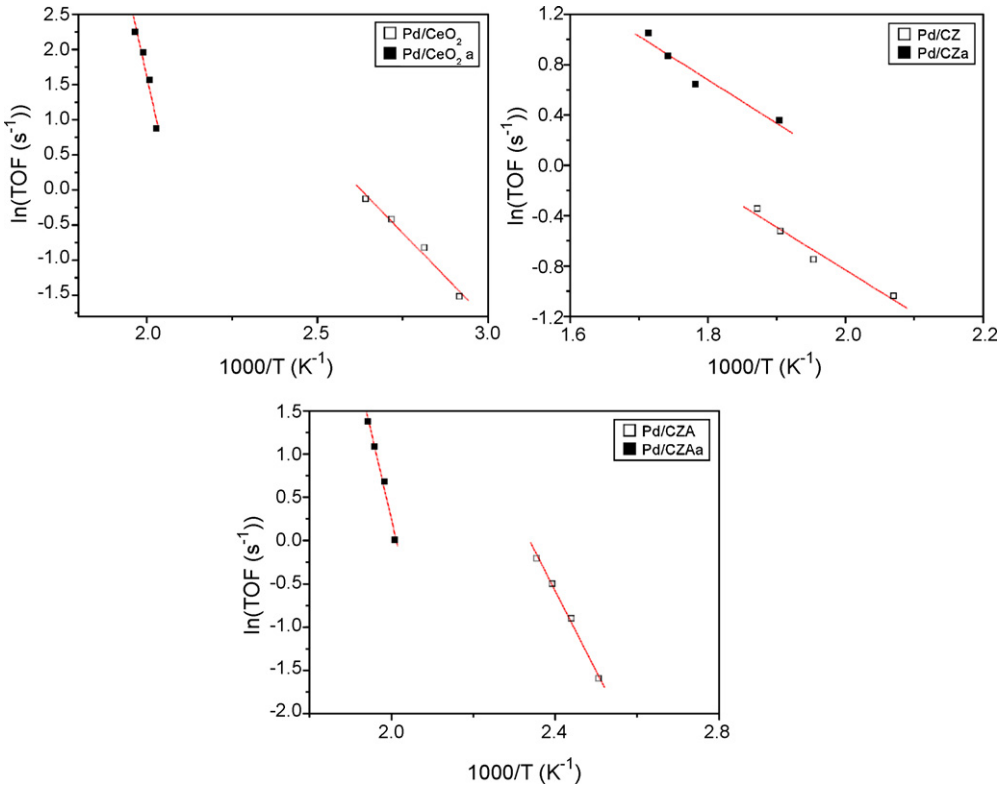

Fig. 6. Arrhenius plots interpreted as turnover frequency (TOF) for WGS reactions for different catalysts.

cycle. DOSR can be calculated as:

$$\text{DOSR} = \int_0^1 \text{CO}_2 \text{ signal} = \text{Rate}\,[\mu\text{mol CO}_2\,\text{s}^{-1}]$$

where $\int_0^1 \text{CO}_2$ signal is the integrated CO_2 peak area from 0 to 1 s.

As is shown in Table 2, the DOSR is generally in the order of Pd/CZA > Pd/CZ > Pd/CeO_2. The data suggests that the specific surface areas are not the only limiting factor for the DOSCs. According to the literature, it is inferred that the Eley–Rideal pathway for CO oxidation is more likely to take place at the initial 0–1 s of CO pulse, where gaseous CO reacts with surface oxygen on the solid surface to form the desorbed gas CO_2 [33]. So the higher concentration of surface oxygen is the key factor for improved DOSR. Although CeO_2 has the highest of surface oxygen concentration associated with Ce^{4+} sites, the introduction of Zr and Al improves the rate of oxygen migration and the extent of oxygen utilization. After hydrothermal ageing treatment, the DOSR decreases due to the sintering of PM particles and agglomeration of support oxides. According to the literature [33], catalysts with smaller crystallite size have higher DOSR, because more surface oxygen can be supplied for CO reaction. As Pd/CZAa has the smallest crystallite size, it has the higher DOSR than that of the others.

3.3. WGS reaction analysis

WGS significantly contributes to CO conversion when steam is present in automobile exhaust. Another important function of the WGS reaction is producing H_2, which has superior activity for NO_x reduction.

WGS activity was evaluated in a gas mixture of CO, H_2O, and N_2. The conversion profiles are shown in Fig. 5. T_{50} for 50% conversion of reactant was used for comparison. The lower the T_{50}, the higher the activity of catalyst has. As shown in Fig. 5, for the fresh samples, T_{50} is as follows: Pd/CeO_2 (182 °C) < Pd/CZA (212 °C) < Pd/CZ (338 °C). After hydrothermal ageing, the order of the T_{50} is Pd/CZA (290 °C) < Pd/CeO_2 (298 °C) < Pd/CZ (393 °C). Previous literatures reported that ceria plays an important role in WGS reactions [12,13]. Higher content of active ceria species is crucial for this. So the fresh Pd/CeO_2 sample shows better activity to other samples. After hydrothermal ageing, large amount of ceria components have become deactivated. As shown in Fig. 5, Pd/CZAa shows the best activity compared with others due to the better thermal stability. Moreover, as reported by Panagiotopoulou et al. [14], the improved WGS activity also depends on the well dispersion of PM particles. Being promoted by the active PM particles, the WGS activity is enhanced through increasing reducing capability of the surface ceria patches in proximate contact with PM particles. The variations of WGS activities are the synergetic effect of these two factors.

To make precise comparisons by normalizing the reaction rate to surface Pd atoms, the turnover frequency (TOF) were calculated as [34,35]:

$$\text{TOF}\,(\text{s}^{-1}) = \frac{X}{100}\left(\frac{dN_{\text{CO}}}{dt}\right)\left(\frac{1}{N_A^{\text{Pd}}}\right),$$

where X is the conversion in %, and (dN_{CO}/dt) is the number of inlet CO molecules per second. N_A^{Pd} is the number of surface Pd atoms, which can be calculated by $N_A^{Pd} = m_{cat}x_{Pd}D_{Pd}N_A/M_{Pd}$, where m_{cat} is the mass of the catalyst, x_{Pd} is the Pd loading in the catalyst expressed in fraction ($x_{Pd} = 0.005$), and D_{Pd} is the palladium dispersion, $N_A = 6.022 \times 10^{23}$ mol^{-1}, $M_{Pd} = 106.4$ g mol^{-1}. According to the research findings of Boudart et al. [34], the TOF at low conversions ($X < 15\%$) are related to the reaction rate. The calculated TOF values can be plotted in Arrhenius coordinates, i.e. ln(TOF) versus $1/T$ (K). The results for all samples are presented in Fig. 6. Fitting reaction rate data to the Arrhenius equation gave the pre-exponential factors and activation energies. As listed in Table 3, Pd/CZ sample shows the lowest activation energy, demonstrating its superior cat-

Table 3
Apparent activation energy and the Arrhenius pre-exponential factor for WGS reaction of fresh and aged Pd supported samples[a].

Samples	E_a (kJ mol^{-1})		ln A	
	Fresh	Aged	Fresh	Aged
Pd/CeO_2	41.7 ± 4.1	182.5 ± 31.0	13.2 ± 1.4	45.5 ± 7.4
$Pd/Ce_{0.67}Zr_{0.33}O_2$	28.1 ± 3.8	28.7 ± 5.2	5.9 ± 0.9	6.9 ± 1.1
$Pd/Ce_{0.67}Zr_{0.33}O_2$-Al_2O_3	76.7 ± 3.9	169.8 ± 15.1	21.6 ± 1.1	41.1 ± 3.6

[a] The kinetic parameters are calculated from a linear regression, and the error intervals are provided.

alytic activity for WGS reaction. As suggested by Ricote et al. [15], the rate-determining step has been proposed to be the decomposition of surface formate. Interestingly, both H_2O and type/loading of the metal promoter (e.g. Zr) have been identified to be facilitating formate decomposition. The latter is attributed to the enhanced hydrogen abstraction rate during cleaving process of the formate C–H bond. Furthermore, oxygen vacancies in ceria are involved in the generation of the active sites for WGS [11]. After the introduction of Zr and Al, charge compensation and radius effect of Zr and Al insertion will disturb the charge equilibrium and distort the cubic fluorite structure, resulting in the oxygen vacancies formation associated with Ce^{3+} sites, in which H_2O dissociation occurred. According to Wang et al. [16], the WGS reaction on Pd/ceria appears to have a bifunctional mechanism: ceria supplies [O] from water to Pd sites, and promotes subsequent CO oxidation. So WGS reaction rates are in positive correlation with the higher Pd surface areas. As Pd/CZ sample has the highest Pd surface area, the catalyst shows superior WGS reaction rates.

After hydrothermal ageing, the activation energy increased. PM and support sintered during the ageing, and thus suppressed the WGS activity. According to Ruettinger et al. [17], the deactivation of WGS reaction is ascribed to the decline of PM dispersion. According to the research findings of Wang et al. [16], stabilizing the WGS activity of ceria-based catalyst requires the good maintaining of metal dispersion during the ageing. It is clear that Pd/CZ has the most limited loss of precious metal dispersion among the aged samples.

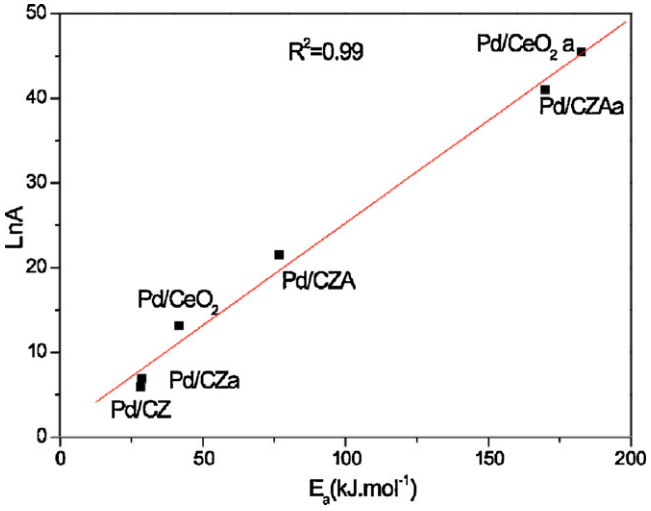

Fig. 7. Illustration of compensation effect for WGS reactions over different catalysts.

As listed in Table 3, the activation energies of different samples are inconsistent with their overall ranking of catalytic performances. This contradiction is induced by the compensation effect [36]. The linear correlation between E_a and ln A for the catalysts is plotted in Fig. 7. For each reactant, if the data points for each catalyst are lying on the same straight line, it means that, for the specific reactant, these catalysts share the same reaction path on the same kind of active centers. As shown in Fig. 7, the points can

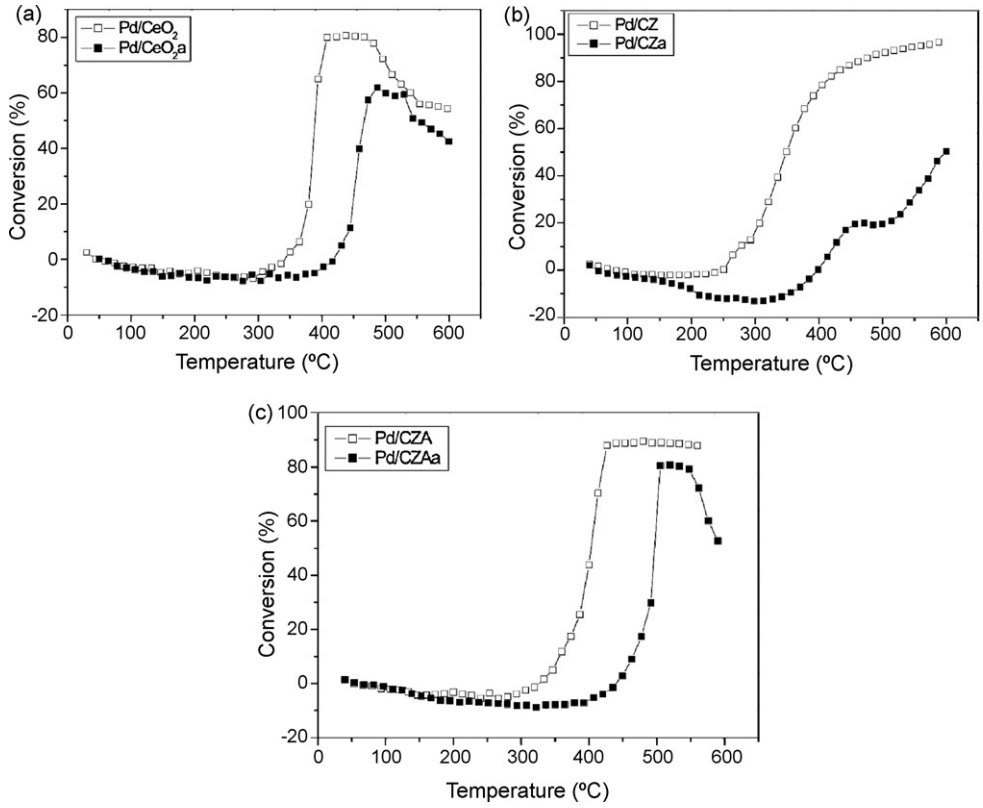

Fig. 8. Conversion profiles of steam reforming over (a) Pd/CeO_2, (b) $Pd/Ce_{0.67}Zr_{0.33}O_2$ and (c) $Pd/Ce_{0.67}Zr_{0.33}O_2$-Al_2O_3 catalysts.

be fitted into a line with limited errors, suggesting the catalysts we investigated share same WGS mechanism. It is conjectured that the reactants are weakly chemisorbed (possibly with a low surface coverage), and the changes of E_a may be caused by different adsorption enthalpies, which cannot fully reflect the overall catalytic activities.

3.4. SR reaction analysis

Hydrocarbon steam reforming reactions can intervene the TWC reaction network as a reducing medium, and may amplify the stoichiometric window. According to the literatures [9,18], the chemical valence of PM particles and the surface basicity of support oxides are the two major factors that determine the SR reaction efficiency. SR activities were evaluated in a gas mixture of C_3H_8, H_2O, and N_2. The conversion profiles are shown in Fig. 8.

For fresh samples, T_{50} is ordered as Pd/CZ (347 °C) < Pd/CeO_2 (389 °C) < Pd/CZA (402 °C). After hydrothermal ageing, T_{50} is increased mainly due to the sintering of PM particles. The order of T_{50} is Pd/CeO_2 (467 °C) < Pd/CZA (497 °C) < Pd/CZ (599 °C). It appears that palladium oxides were the most active phase for the SR reaction. Several literatures have shown a close correlation between the deactivation of the catalyst and the decomposition of the palladium oxides [9,19]. Previously studies suggest that there are two different chemical states of the palladium oxides: (i) easily reducible PdO covering metal particles, and (ii) stable bulk oxides in close contact with alumina, which is also considered as the isolated palladium aluminate [9]. Moreover, the discrepancy of catalytic activities can also be ascribed to the different acid strength of support oxides, because surface acidity is a vital factor to control the oxidation states of Pd particles [37]. The lower activity of Pd/CZA possibly attributes to the formation of palladium–aluminum bonding, making the Pd particles less oxidative. According to the findings of Feio et al. [20], the catalytic activities of Pd/CeO_2-Al_2O_3 catalysts in the steam reforming positively depend on CeO_2 content. So the Pd/CeO_2 catalysts show a lower T_{50}. According to the findings of Colussi et al. [21], CeO_2 is a very effective promoter for Pd re-oxidation, resulting in a strong reduction of the Pd–PdO hysteresis, which has been recognized as the active coupling sites for alkane oxidation.

Table 4
Apparent activation energy and the Arrhenius pre-exponential factor for SR reaction of fresh and aged Pd supported samples[a].

Samples	E_a (kJ mol^{-1})		ln A	
	Fresh	Aged	Fresh	Aged
Pd/CeO_2	238.0 ± 23.5	303.0 ± 28.4	41.5 ± 4.4	50.3 ± 4.8
Pd/$Ce_{0.67}Zr_{0.33}O_2$	104.2 ± 25.9	248.4 ± 30.5	19.4 ± 5.7	41.0 ± 5.3
Pd/$Ce_{0.67}Zr_{0.33}O_2$-Al_2O_3	207.5 ± 9.6	323.2 ± 30.8	36.5 ± 1.8	51.1 ± 5.1

[a] The kinetic parameters are calculated from a linear regression, and the error intervals are provided.

Kinetic analysis for SR reactions was carried out as that for WGS reactions. The Arrhenius plot for the TOF of SR was shown in Fig. 9. Fitting reaction rate to Arrhenius equation gave the pre-exponential factors and activation energies. As listed in Table 4, the E_a of Pd/CZ is the lowest, in agreement with the activity test results. However, the E_a of the aged samples is inconsistent with the order of their overall catalytic performances. The compensation effect was considered. The linear correlation between E_a and ln A for each reactant is plotted. As shown in Fig. 10, for the specific reactants, the points representing the different samples fit into a line with limited error, suggesting that all the catalysts share the very similar reaction mechanism. Propane steam reforming is suggested to be containing the following steps [18]. First, propane molecule is dissociatively adsorbed on Pd particles, and H_2O is made active by the support oxides at the same time. Then, hydroxyl species migrate to Pd particles to react with CH_x fragments, producing carbon oxides and hydrogen through the dissociation.

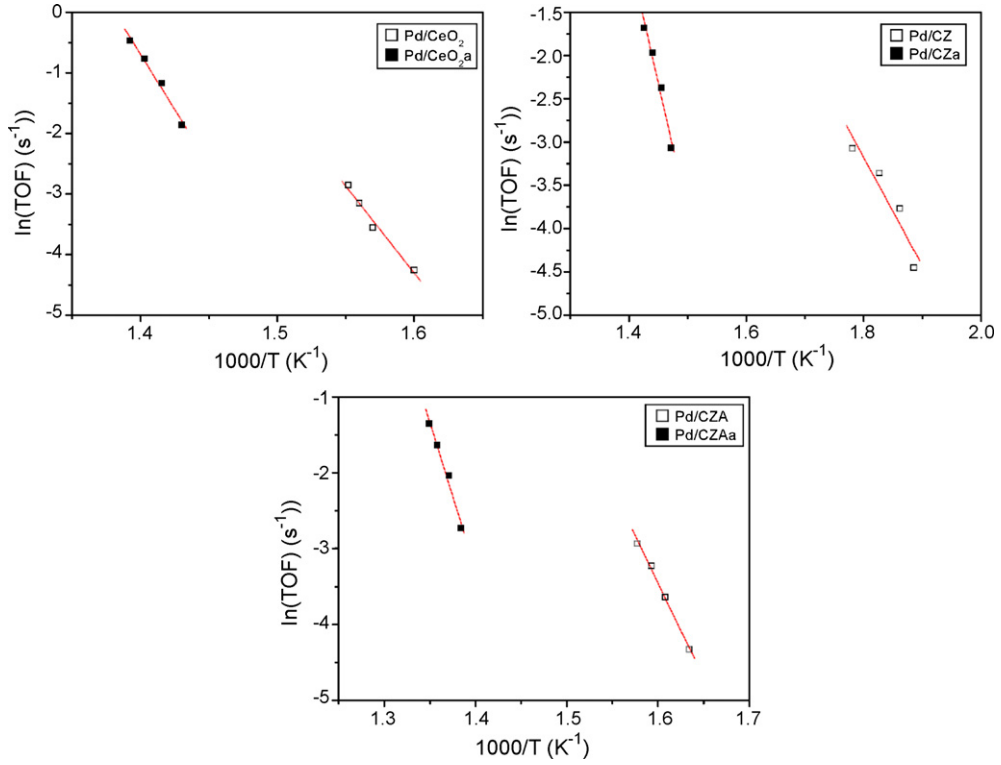

Fig. 9. Arrhenius plot interpreted as turnover frequency (TOF) of SR reactions over different catalysts.

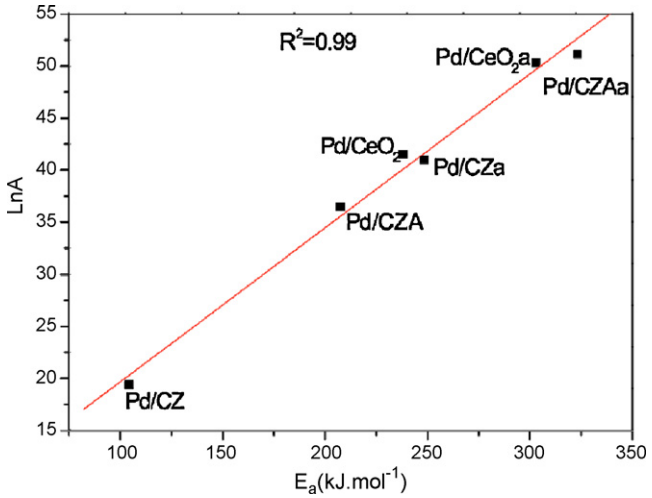

Fig. 10. Illustration of compensation effect for SR reactions over different catalysts.

4. Conclusion

The performances for oxygen storage capacity, water–gas shift and steam reforming reactions over Pd/CeO_2, $Pd/Ce_{0.67}Zr_{0.33}O_2$, and $Pd/Ce_{0.67}Zr_{0.33}O_2$-Al_2O_3 three-way catalysts have been compared. The major driving forces for the different catalytic activities have been discussed. From kinetic analysis, the confirmation of compensation effect revealed that all catalysts share the same mechanism for the separated reactions we investigated.

For OSC reactions, the introduction of Zr and Al into ceria lattice improves the oxygen mobility. Although the ceria contents should be lower in Zr and Al introduced samples, much higher responding rate for oxygen release and uptake has been observed. WGS activity depends on the synergetic effect of ceria contents, oxygen vacancies, and precious metal dispersions. Therefore, although $Pd/Ce_{0.67}Zr_{0.33}O_2$ has the lowest activation energy for WGS, Pd/CeO_2 and $Pd/Ce_{0.67}Zr_{0.33}O_2$-Al_2O_3 have the lowest T_{50} in fresh and aged states respectively. Oxidized states of palladium particles and less acidity of support oxides are the two major factors contributing for better SR reaction activity. The $Pd/Ce_{0.67}Zr_{0.33}O_2$ and Pd/CeO_2 have the lowest T_{50} for SR in fresh and aged states respectively, and $Pd/Ce_{0.67}Zr_{0.33}O_2$ has the lowest activation energy for the SR reactions.

Acknowledgements

The authors are grateful to the financial support from the Program of New Century Excellent Talents in University (NCET-06-0243), the Program of Natural Science Foundation of China (No. 50972104), and the Program of Introducing Talents of Discipline to Universities of China (No. B06006).

References

[1] R. Di Monte, J. KaŠpar, Top. Catal. 28 (2004) 47.
[2] A. Trovarelli, Catal. Rev. Sci. Eng. 38 (1996) 439.
[3] T. Murota, T. Hasegawa, S. Aozasa, et al., J. Alloys Compd. 193 (1993) 298.
[4] R. Di Monte, P. Fornasiero, S. Desinan, et al., Chem. Mater. 16 (2004) 4273.
[5] A. Morikawa, T. Suzuki, T. Kanazawa, et al., Appl. Catal. B: Environ. 78 (2007) 210.
[6] M.W. Zhao, M.Q. Shen, J. Wang, J. Catal. 248 (2007) 258.
[7] T. Maillet, J. Barbier Jr., D. Duprez, Appl. Catal. B: Environ. 9 (1996) 251.
[8] L. Pino, A. Vita, F. Cipiti, et al., Appl. Catal. A: Gen. 306 (2006) 68.
[9] T. Maillet, C. Solleau, J. Barbier Jr., Appl. Catal. B: Environ. 14 (1997) 85.
[10] A.M. Pisanu, C.E. Gigola, Appl. Catal. B: Environ. 11 (1996) L37.
[11] X.Q. Wang, J.A. Rodriguez, J.C. Hanson, et al., J. Phys. Chem. B 110 (2006) 428.
[12] J. Barbier Jr., D. Duprez, Appl. Catal. B: Environ. 4 (1994) 105.
[13] P.S. Querino, J.R. Carlos Bispo, M. do Carmo Rangel, Catal. Today 107–108 (2005) 920.
[14] P. Panagiotopoulou, J. Papavasiliou, G. Avgouropoulos, et al., Chem. Eng. J. 134 (2007) 16.
[15] S. Ricote, G. Jacobs, M. Milling, et al., Appl. Catal. A: Gen. 303 (2006) 35.
[16] X. Wang, R.J. Gorte, J.P. Wagner, J. Catal. 212 (2002) 225.
[17] W. Ruettinger, X.S. Liu, R.J. Farrauto, Appl. Catal. B: Environ. 65 (2006) 135.
[18] X. Wang, R.J. Gorte, Appl. Catal. A: Gen. 224 (2002) 209.
[19] S. Specchia, E. Finocchio, G. Busca, et al., J. Catal. 263 (2009) 134.
[20] L.S.F. Feio, C.E. Hori, S. Damyanova, Appl. Catal. A: Gen. 316 (2007) 107.
[21] S. Colussi, A. Trovarelli, G. Groppi, et al., Catal. Commun. 8 (2007) 1263.
[22] M. Alifanti, B. Baps, N. Blangenois, et al., Chem. Mater. 15 (2003) 395.
[23] J. Wang, J. Wen, M.Q. Shen, J. Phys. Chem. C 112 (2008) 5113.
[24] R. Di Monte, J. Kaspar, P. Fornasiero, et al., Inorg. Chim. Acta 334 (2002) 318.
[25] E. Aneggi, J. Llorca, M. Boaro, J. Catal. 234 (2005) 88.
[26] H. Vidal, J. Kašpar, M. Pijolat, Appl. Catal. B: Environ. 30 (2001) 75.
[27] E. Mamontov, T. Egami, R. Brezny, J. Phys. Chem. B 104 (2000) 11110.
[28] P. Fornasiero, E. Fonda, R. Di Monte, J. Catal. 187 (1999) 177.
[29] C. Bozo, N. Guilhaume, J.-M. Herrmann, J. Catal. 203 (2001) 393.
[30] P.S. Lambrou, C.N. Costa, S.Y. Christou, et al., Appl. Catal. B: Environ. 54 (2004) 237.
[31] C.E. Hori, A. Brenner, K.Y. Simon Ng, et al., Catal. Today 50 (1999) 299.
[32] L.W. Jia, M.Q. Shen, J. Wang, et al., J. Alloys. Compd. 454 (2008) 321.
[33] R.H. Nibbelke, A.J.L. Nievergeld, J.H.B.J. Hoebink, Appl. Catal. B: Environ. 19 (1998) 245.
[34] M. Boudart, G. Ertl, H. Knozinger, J. Weitkamp (Eds.), Handbook of Heterogeneous Catalysis, Verlag Chemie, Weinheim, 1997, p. 958.
[35] A. Wootsch, C. Descorme, S. Rousselet, Appl. Surf. Sci. 253 (2006) 1310.
[36] G.C. Bond, M.A. Keane, H. Kral, et al., Catal. Rev. Sci. Eng. 42 (2000) 323.
[37] Y. Yazawa, H. Yoshida, N. Takagi, et al., J. Catal. 187 (1999) 15.